LETTER

High-Performance Single CdS Nanowire (Nanobelt) Schottky Junction Solar Cells with Au/Graphene Schottky Electrodes

Yu Ye,[†] Yu Dai,[†] Lun Dai,*[,†] Zujin Shi,[‡] Nan Liu,[‡] Fei Wang,[†] Lei Fu,[‡] Ruomin Peng,[†] Xiaonan Wen,[†] Zhijian Chen,[†] Zhongfan Liu,[‡] and Guogang Qin*[,†]

State Key Lab for Mesoscopic Physics and School of Physics, Peking University, Beijing 100871, China, and College of Chemistry and Molecular Engineering, Peking University, Beijing 100871, China

ABSTRACT High-performance single CdS nanowire (NW) as well as nanobelt (NB) Schottky junction solar cells were fabricated. Au (5 nm)/graphene combined layers were used as the Schottky contact electrodes to the NWs (NBs). Typical as-fabricated NW solar cell shows excellent photovoltaic behavior with an open circuit voltage of ~0.15 V, a short circuit current of ~275.0 pA, and an energy conversion efficiency of up to ~1.65%. The physical mechanism of the combined Schottky electrode was discussed. We attribute the prominent capability of the devices to the high-performance Schottky combined electrode, which has the merits of low series resistance, high transparency, and good Schottky contact to the CdS NW (NB). Besides, a promising site-controllable patterned graphene transfer method, which has the advantages of economizing graphene material and free from additional etching process, was demonstrated in this work. Our results suggest that semiconductor NWs (NBs) are promising materials for novel solar cells, which have potential application in integrated nano-optoelectronic systems.

KEYWORDS: graphene • solar cells • Schottky junction • nanowire • nanobelt • CdS

INTRODUCTION

Solar cells, which convert solar energy into electrical energy with respectable conversion efficiencies, are attractive candidates for clean and renewable power sources (1, 2). The widespread concern about energy sources (3, 4) has created a lot of efforts to explore solar cells. For example, organic (5, 6), hybrid organic−inorganic (7, 8), all-inorganic (9), and dye-sensitized (10, 11) solar cells have been developed. With the possibility of serving as integrated power sources for nano-optoelectronic systems, semiconductor single nanowire (NW) or nanobelt (NB) solar cells have attracted intense attention (8, 12−16). So far, two critical parameters, which limit the application of these new concept solar cells, are energy conversion efficiency and cost. Lieber's group reported axial *p-i-n* single Si NW (12), coaxial *p-i-n* single III-nitride NW (13), and coaxial *p-i-n* single Si NW (14) solar cells with efficiencies of 0.5, 0.19, and 3.4%, respectively. However, the high cost and complication of the material fabrication involved may limit the device application. Recently, Yang's group reported a polymer/ZnO hybrid single NW solar cel l (8) with an efficiency of 0.036%. Schottky junction is another alternative structure for the photovoltaic (PV) device. Basically, any semiconductor can form a Schottky junction with a certain metal if their work function difference is big enough, and the carrier density of the semiconductor is low or moderate. In addition, the fabrication of Schottky junctions has the merit of low-cost and simplicity. Atwater's group reported Si NW Schottky solar cell with an efficiency of 0.46% (15). However, their devices were realized by destroying a certain part of the NW via applying an extremely high current density (>10 kA cm^{-2}). The method was less reliable, and the nature of the induced junction was not explicitly understood yet. Previously, we had reported the CdS NB Schottky junction PV devices (16) by using microfabrication processes compatible with Si microelectronic integration. However, therein, the Schottky contact Au film (100 nm) had absorbed most of the simulated solar energy. Rather, we found that reducing the Au film thickness to 50 nm (corresponding transparency <10%) would render a marked degradation of the performance of the CdS NB/Au Schottky junction (16). Therefore, the performance of our previous PV devices was greatly limited.

It is well-known that graphene has the merit of high carrier mobility (17), remarkable conductivity (18), and transparency (19). It has potential application in making novel electronic (20−22) and optoelectronic devices (23, 24). In this letter, we report the realization of high-performance single CdS NW (NB) Schottky junction solar cells by employing Au (5 nm)/graphene combined electrodes. The combined electrodes have high transparency (>74%) of solar spectrum and can form good Schottky contact to the CdS NW (NB). The physical mechanism of the combined Schottky electrode is discussed. The as-fabricated single NW solar cells exhibit high efficiency of ~1.65%. A novel site-controllable patterned graphene transfer method was developed. Compared

* Corresponding author. E-mail: lundai@pku.edu.cn (L.D.); qingg@pku.edu.cn (G.Q.).

Received for review August 20, 2010 and accepted November 1, 2010

[†] State Key Lab for Mesoscopic Physics and School of Physics, Peking University.

[‡] College of Chemistry and Molecular Engineering, Peking University.

DOI: 10.1021/am1007672

Published on Web 11/08/2010

to the commonly used graphene patterning method, which involves large-scale graphene transfer and etching process, herein, the site-controllable patterned graphene transfer method has the merits of economizing graphene material and free from additional etching process. This approach is of special benefit to experimental fabrication of randomly distributed NW (NB) devices. Both the site-controllable patterned graphene transfer approach and the graphene based combined electrode concept in this work can be easily applied to diverse devices.

EXPERIMENTAL SECTION

Both the *n*-CdS NWs (NBs) (25) and the graphene used in this work were synthesized via the chemical vapor deposition method. For synthesis of graphene, a 300 nm Ni film catalyst was deposited on Si/SiO_2 substrates by direct current magnetron sputtering (Gamma 1000C sputtering system). The as-prepared substrates were placed onto a quartz boat, which was later inserted into the center of a quartz tube placed in a tube furnace. The furnace was heated to 1000 °C in 40 min under a hybrid flow of H_2 (50 SCCM) and Ar (250 SCCM). When the temperature reached 1000 °C, a reaction gas mixture of CH_4, H_2, and Ar with flow rates of 25, 50, and 250 SCCM, respectively, was let into the quartz tube for 3 min. After that, the furnace was rapidly cooled to room temperature at a rate of 10 °C s^{-1} in the Ar ambient.

The as-synthesized graphenes were transferred by the stamp method with the help of PMMA (poly methyl methacrylate) (26) to Si/400 nm SiO_2 substrates for Raman and electrical property characterization, and transferred to quartz substrates with and without thermally evaporated Au (5 nm) for transparency characterization. Raman measurement was performed with a microzone confocal Raman spectroscope (Renishaw inVia microRaman system) equipped with a color charge-coupled (CCD) device. The excitation wavelength was 514 nm. The electrical property was measured by a Hall measurement system (Accent HL5500). The transparency was measured by a UV−vis−NIR recording spectrophotometer (Shimadzu UV-3100).

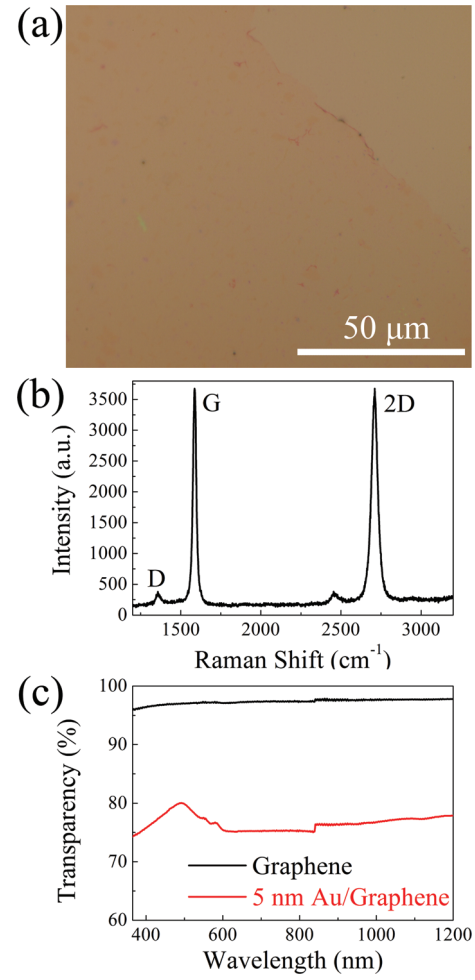

FIGURE 1. (a) Optical microscope image of the graphene film on a Si/SiO_2 substrate. (b) Raman spectrum of the graphene film depicted in panel a. (c) Transparency spectra of a graphene film and a 5 nm Au/graphene film both on quartz substrates.

RESULTS AND DISCUSSION

Figure 1a shows a typical optical image of the graphene on a Si/SiO_2 substrate taken by an optical microscope (Olympus BX51M). We can see that the graphene is continuous and clean. Typical Raman spectrum (Figure 1b) of as-synthesized graphene shows two main peaks: a narrow line width (~26 cm^{-1}) G-band peak (~1586 cm^{-1}) and a narrow line width (~46 cm^{-1}) 2D-band peak (~2710 cm^{-1}). Their intensity ratio (I_{2D}:I_G) is about 1, indicating the formation of bilayer graphene. Besides, the defect-related (27) D-band peak (~1355 cm^{-1}) is weak, indicating the high quality of the graphene.

Figure 2a−e shows a schematic illustration of the fabrication and transfer processes of the patterned graphenes used in the single NW (NB) solar cells. First, a layer of PMMA was spun on the graphene synthesized on a Si/SiO_2/Ni substrate (Figure 2a). Then electron beam lithography (EBL) (FEI Strata DB 235) was employed to pattern the PMMA into desired shape (Figure 2b). The lower-left inset in Figure 2b shows the magnified "violoncello" shaped PMMA used in our case. Then, the PMMA patterns together with the underlying graphene were separated from the Si/SiO_2 substrate by etching the Ni layer with $FeCl_3$ solution (1M) (Figure 2c). The lower-left inset shows a zoom-in picture of the graphene/patterned PMMA layers after removing the underlying Ni layer. After transferring the graphene/patterned PMMA layers to another Si/SiO_2 substrate, we used two glass probes to insert into the two holes of a "violoncello" shaped PMMA, lifted it off together with the underlying graphene (Figure 2d), and transferred them onto the desired place on a device substrate under an optical microscope. In our case, they were transferred onto a NW (NB) covered by 5 nm Au layer in between two In/Au (10/100 nm) ohmic contact electrodes on a Si/SiO_2 substrate. A process of heat treatment (120 °C, 30 min) in oven was carried out for better electrical contact of the graphene with the NW (NB). After that, the PMMA was removed with acetone. Finally, an Au (100 nm) ohmic contact electrode was defined on the graphene away from the NW (NB), which was used for welding the connecting Al wire (Figure 2f). In this work, all the metal layers were fabricated with UV photolithography followed by thermal evaporation and lift-off processes.

A typical field-emission scanning electron microscope (FESEM) (FEI Strata DB 235) image of an as-fabricated single NW solar cell is shown in Figure 3a. The outline of the "violoncello" shaped graphene is highlighted with white

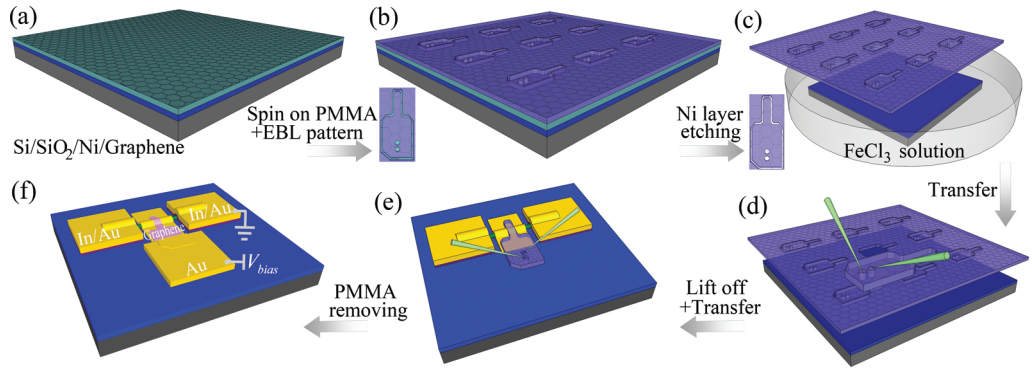

FIGURE 2. (a−e) Schematic illustration of the fabrication and transfer processes of the patterned graphenes used in the single NW(NB) solar cells. (a) Synthesizing a large-scale graphene film on a Si/SiO_2/Ni substrate. (b) Layer of PMMA is spun on the synthesized graphene and then patterned by EBL into desired shape. The lower-left inset shows the magnified "violoncello"-shaped PMMA used in our case. (c) The PMMA patterns together with the underlying graphene are separated from the Si/SiO_2 substrate by etching the Ni layer with $FeCl_3$ solution (1 M). The lower-left inset shows a zoom-in picture of the graphene/patterned PMMA layers after removing the underlying Ni layer. (d) Transferring the graphene/patterned PMMA layers to another Si/SiO_2 substrate, and lifting a "violoncello"-shaped PMMA together with the underlying graphene off by two glass probes under an optical microscope. (e) Transferring them onto a NW (NB) covered by 5 nm Au layer in between two ohmic contact electrodes on a device substrate. (f) After the heat treatment, removing the PMMA with acetone, and fabricating an Au (100 nm) ohmic contact electrode on the graphene away from the NW (NB).

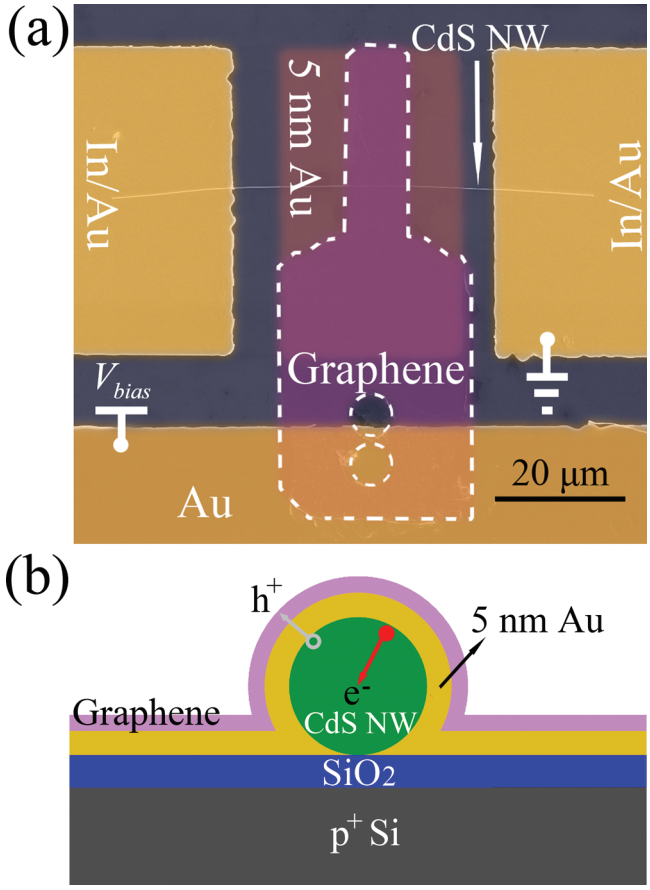

FIGURE 3. (a) Typical FESEM image of an as-fabricated single NW solar cell. (b) Cross-sectional view around the junction of the device.

dashed lines. The width of the graphene on the CdS NW and the diameter of CdS NW are about 10 μm and 100 nm, respectively. Figure 3b shows the cross-sectional view around the junction of the device. The photogenerated holes (h^+) and electrons (e^-) are driven toward the Schottky electrode (Au/Graphene layer) and CdS NW, respectively, by the built-in electric field at the Schottky junction.

To discuss the physical mechanism of the combined Schottky electrode and the graphene's effectiveness in it, we have measured the transparencies of the graphene and Au (5 nm)/graphene layers in the 400−1200 nm wavelength range as shown in Figure 1c. The corresponding values are above 97% and 74%, respectively. Furthermore, we have employed Hall measurement to characterize the conductivity of the 5 nm Au, the graphene and the Au (5 nm)/graphene combined electrode. It is worth noting that in all measurements, ohmic contact Au pads (100 nm) were deposited on the measured thin films for the welding or the probing processes. The measured sheet resistances of the 5 nm Au, graphene, and Au (5 nm)/graphene layers are about 1.8×10^{10}, 2224, and 410 Ω/□, respectively. From these results, we can see that the conductivity of 5 nm Au is too small to be used as an effective electrode layer. On the other hand, although the transparencies of the graphene is higher than that of Au (5 nm)/graphene layers, the graphene itself can not be used as a Schottky electrode to CdS NW (NB) due to the small work function difference between them (28). Therefore, in our case, the effective Schottky electrode is the Au (5 nm)/graphene layers. Here, the graphene contributes to its conductivity and transparency, and the 5 nm Au layer contributes to its Schottky contact to the CdS NW (NB). Overall, the combined electrode, which taking advantages of both the high-quality graphene and high-work-function Au thin film, has the merits of low series resistance, high transparency, and good Schottky contact to the CdS NW (NB).

The mechanism of a Schottky junction solar cell can be understood qualitatively by plotting the energy band diagram. Figure 4a shows energy diagram of a forward-biased single CdS NW (NB) Schottky junction solar cell under illumination. Because Au and the graphene can form good ohmic contact with each other, no clear potential barrier is formed at their interface. However, due to the work function difference between the Au (Φ_{Au} ~5.37 eV) and CdS (Φ_{CdS} ~5.0 eV) (29) and the lower electron density of the CdS, a

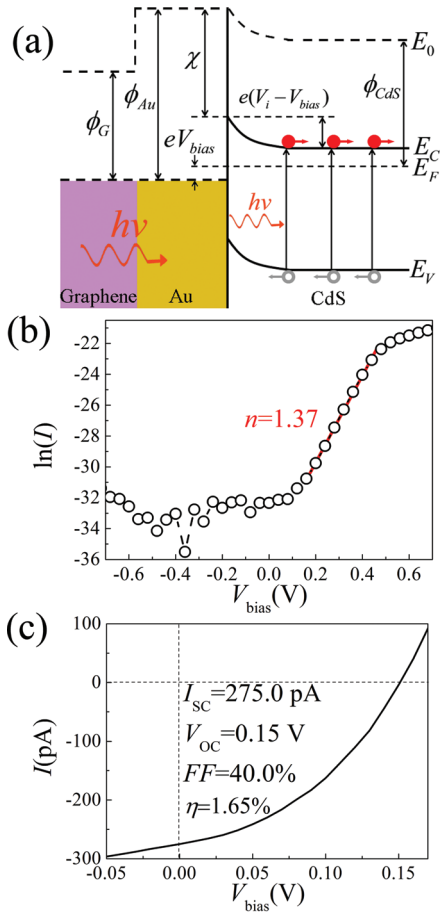

FIGURE 4. (a) Energy diagram of a forward-biased single CdS NW (NB) Schottky junction solar cell under illumination. Φ_G, Φ_{Au}, Φ_{CdS} are the work functions of graphene, Au, and CdS, respectively. eV_i is the built-in potential. V_{bias} is the forward-biased voltage. χ is the electron affinity of CdS. E_C, E_V, E_F correspond to the conduction band edge, valence band edge, and Fermi level of CdS, respectively. E_0 corresponds to the vacuum level. (b) Room-temperature $I-V$ characteristic (in dark) of the single NW solar cell depicted in Figure 3a on a semilog scale. The red straight line shows the fitting result of the $I-V$ curve by the equation $\ln(I) = eV/nkT + \ln(I_0)$. (c) Room-temperature $I-V$ characteristic of the same solar cell under the AM 1.5G illumination.

built-in potential (eV_i) forms in the CdS near the Schottky junction interface. Under illumination, the photogenerated carriers will be separated by the built-in field, and diffuse to the opposite electrodes. When the solar cell is open-circuited, the separation of photogenerated electrons and holes will produce an open circuit voltage V_{OC}. When the solar cell is short-circuited, the extracted photogenerated carriers will transit through the external circuit, generating a short circuit current I_{SC}.

Figure 4b shows the typical room-temperature $I-V$ characteristic (in dark) of the single NW solar cell depicted in Figure 3a on a semilog scale. The electrical transport measurements were done with a semiconductor characterization system (Keithley 4200). During the measurement, one In/Au ohmic contact electrode was grounded, the other one was suspended (please refer to Figure 3a). We can see that the $I-V$ curve shows an excellent rectification characteristic. An on/off current ratio of $\sim 1 \times 10^5$ can be obtained when the voltage changes from +0.7 to −0.7 V. The turn-on voltage is around 0.4 V. For Schottky barrier diodes made with high-mobility semiconductors, such as Si and CdS etc., the current I is determined by the thermionic emission of electrons and can be described by the equation $I = I_0[\exp(eV/nkT) - 1]$ (30), where I_0 is the reverse saturation current, e is the electronic charge, V is the applied bias, n is the diode ideality factor, k is the Bolzmann's constant, and T is the absolute temperature. By fitting the measured $I-V$ curve with the above equation, we obtain $n = 1.37$. Here, n is quite close to that reported for the CdS NB/100 nm Au Schottky junction (16). These results indicate that the combined Au (5 nm)/graphene electrode has formed an excellent Schottky contact with the CdS NW.

Figure 4c shows the typical room-temperature $I-V$ characteristic of the single NW solar cell (depicted in Figure 3a) under air mass (AM) 1.5 global (1.5G) illumination. A solar simulator (Newport 91160−1000) with a calibrated illumination light power density of 100 mW · cm^{-2} was used. This cell exhibits an open circuit voltage (V_{OC}) of about 0.15 V, a short-circuit current (I_{SC}) of about 275.0 pA, a fill factor of about 40.0 %, and a maximum output power (P_{MAX}) of about 16.5 pW. When we estimate the energy conversion efficiency (η), the effective Schottky junction area is used as the projected active light collection area (12, 13), which is the product of the width ($\sim 10\,\mu$m) of the Au (5 nm)/graphene combined electrode and the NW diameter (100 nm). The effective Schottky junction area does not include the area of Au uncovered by the graphene layer, since we have demonstrated that the conductivity of 5 nm Au is too small (i.e., the corresponding series resistance is too big) to be used as the effective electrode. Therefore, $\eta = FFI_{SC}V_{OC}/(P_{in}S) = 1.65\,\%$ (P_{in}, illumination light power density, 100 mW/cm^2; S, effective Schottky junction area). This value is the second best one reported so far for the single NW (NB) solar cells (8, 12−16).

Notably, the as-fabricated devices show excellent environmental stability. Figure 5a shows $I-V$ curves of a CdS NW solar cell (with effective Schottky junction area of ~175 nm $\times 10\,\mu$m) before and after being stored in air for 6 months. We can see that the I_{SC} remained almost unchanged, while the V_{OC} increased from 0.160 to 0.174 V during this period. The slight increase of V_{OC} for CdSe/CNTs Schottky junction solar cells after being stored in air for some time had been observed before by Cao's group (31).They accounted it to the p-doping of CNTs by oxygen adsorption. We think that the slight increase of V_{OC} for our CdS/Au/graphene Schottky junction solar cells may come from the same kind of reason, because Dai's group had reported the phenomenon of p-doping of graphene by the oxygen molecules in air (32). Figure 5b shows a family of the $I-V$ curves of a CdS NB solar cell (with effective Schottky junction area of $\sim 1.27\,\mu$m × $28.75\,\mu$m) during a 10 h illumination process. The I_{SC} remained almost unchanged during the whole measurement process. However, the V_{OC} changed from 0.182 to 0.154 V under the first 5 min illumination. The decreasing of the V_{OC} at the very beginning can be attributed to the illumination heating effect of the cell. It is well-known that there is a

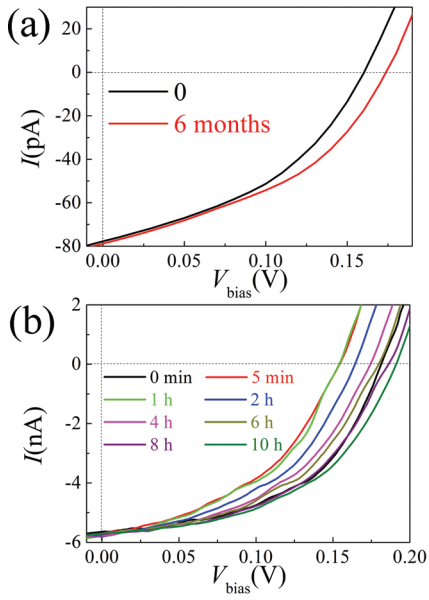

FIGURE 5. The stability test of the single CdS NW (NB) Schottky junction solar cells. (a) *I*−*V* characteristics of a CdS NW cell before and after being stored in air for 6 months. (b) Family of *I*−*V* curves of a CdS NB cell during a 10 h illumination under the AM 1.5G illumination.

negative gradient of dV_{OC}/dT for solar cells (33, 34). Moreover, it is interesting to see that after about 1 h, the V_{OC} began to increase. For instance, from 1 to 10 h illumination process, the V_{OC} increases monotonically from 0.154 to 0.191 V, resulting in an increase of η from 1.06% to 1.47%. The slight increase of V_{OC} and η under long time illumination may also be attributed to *p*-doping of graphene by oxygen molecules in air (31, 32).

CONCLUSION

In summary, we have fabricated novel single CdS NW (NB) Schottky junction solar cells using Au/graphene Schottky contact combined electrodes. A promising site-controllable patterned graphene transfer method was developed for device fabrication, which has the advantages of economizing graphene material and free from additional etching process. The as-fabricated solar cells show excellent PV behavior with the AM 1.5G energy conversion efficiency up to 1.65%. The high performance of our devices can be attributed to the high-performance Schottky combined electrode used here, which has the merits of low series resistance, high transparency (>74%), and good Schottky contact to the CdS NW (NB). Both the site-controllable patterned graphene transfer approach and the graphene based combined electrode concept in this work can be easily applied to diverse devices. Our results also suggest semiconductor NWs (NBs) are promising materials in making novel solar cells, which have the potential possibility of serving as integrated power sources for nano-optoelectronic systems.

Acknowledgment. This work was supported by the National Natural Science Foundation of China (10774007, 11074006, 10874011, 50732001), the National Basic Research Program of China (2006CB921607, 2007CB613402), and the Fundamental Research Funds for the Central Universities.

REFERENCES AND NOTES

(1) Lewis, N. S. *Science* **2007**, *315*, 798–801.
(2) Grätzel, M. *Nature* **2001**, *414*, 338–344.
(3) Dresselhaus, M. S.; Thomas, I. L. *Nature* **2001**, *414*, 332–337.
(4) Potočnik, J. *Science* **2007**, *315*, 810–811.
(5) Tang, C. W. *Appl. Phys. Lett.* **1986**, *48*, 183–185.
(6) Yoo, S.; Domercq, B.; Kippelen, B. *Appl. Phys. Lett.* **2004**, *85*, 5427–5429.
(7) Huynh, W. U.; Dittmer, J. J.; Alivisators, A. P. *Science* **2002**, *295*, 2425–2427.
(8) Briseno, A. L.; Holcombe, T. W.; Boukai, A. I.; Garnett, E. C.; Shelton, S. W.; Fréchet, J. J. M.; Yang, P. D. *Nano Lett.* **2010**, *10*, 334–340.
(9) Gur, I.; Fromer, N. A.; Geier, M. L.; Alivisatos, A. P. *Science* **2005**, *310*, 462–465.
(10) Law, M.; Greene, L. E.; Johnson, J. C.; Saykally, R.; Yang, P. D. *Nat. Mater.* **2005**, *4*, 455–459.
(11) Bach, U.; Lupo, D.; Comte, P.; Moser, J. E.; Weissörtel, F.; Salbeck, J.; Spreitzer, H.; Grätzel, M. *Nature* **1998**, *395*, 583–585.
(12) Kempa, T. J.; Tian, B. Z.; Kim, D. R.; Hu, J. S.; Zheng, X. L.; Lieber, C. M. *Nano Lett.* **2008**, *8*, 3456–3460.
(13) Dong, Y. J.; Tian, B. Z.; Kempa, T. J.; Lieber, C. M. *Nano Lett.* **2009**, *9*, 2183–2187.
(14) Tian, B. Z.; Zheng, X. L.; Kempa, T. J.; Fang, Y.; Yu, N. F.; Yu, G. H.; Huang, J. L.; Lieber, C. M. *Nature* **2007**, *449*, 885–890.
(15) Kelzenberg, M. D.; Turner-Evans, D. B.; Kayes, B. M.; Filler, M. A.; Putnam, M. C.; Lewis, N. S.; Atwater, H. A. *Nano Lett.* **2008**, *8*, 710–714.
(16) Ye, Y.; Dai, L.; Wu, P. C.; Liu, C.; Sun, T.; Ma, R. M.; Qin, G. G. *Nanotechnology* **2009**, *20*, 375202.
(17) Bolotin, K. I.; Sikes, K. J.; Jiang, Z.; Klima, M.; Fudenberg, G.; Hone, J.; Kim, P.; Stormer, H. L. *Solid State Commun.* **2008**, *146*, 351–355.
(18) Wu, Z. S.; Ren, W. C.; Gao, L. B.; Zhao, J. P.; Chen, Z. P.; Liu, B. L.; Tang, D. M.; Yu, B.; Jiang, C. B.; Cheng, H. M. *ACS Nano* **2009**, *3*, 411–417.
(19) Li, X. S.; Zhu, Y. W.; Cai, W. W.; Borysiak, M.; Han, B. Y.; Chen, D.; Piner, R. D.; Colombo, L.; Ruoff, R. S. *Nano Lett.* **2009**, *12*, 4359–4363.
(20) Fowler, J. D.; Allen, M. J.; Tung, V. C.; Yang, Y.; Kaner, R. B.; Weiller, B. H. *ACS Nano* **2009**, *3*, 301–306.
(21) Lin, Y. M.; Jenkins, K. A.; Valdes-Garcia, A.; Small, J. P.; Farmer, D. B.; Avouris, P. *Nano Lett.* **2009**, *9*, 422–426.
(22) Sordan, R.; Traversi, F.; Russo, V. *Appl. Phys. Lett.* **2009**, *94*, 073305.
(23) Wang, X.; Zhi, L. J.; Müllen, K. *Nano Lett.* **2008**, *8*, 323–327.
(24) Wu, J. B.; Agrawal, M.; Becerril, H. A.; Bao, Z. N.; Liu, Z. F.; Chen, Y. S.; Pumans, P. *ACS nano* **2010**, *1*, 43–48.
(25) Wu, P. C.; Ma, R. M.; Liu, C.; Sun, T; Ye, Y.; Dai, L. *J. Mater. Chem.* **2009**, *19*, 2125–2130.
(26) Reina, A.; Jia, X. T.; Ho, J.; Nezich, D.; Son, H.; Bulovic, V.; Dresselhaus, M. S.; Kong, J. *Nano Lett.* **2009**, *9*, 30–35.
(27) Ferrari, A. C. *Solid State Commun.* **2007**, *143*, 47–57.
(28) Shi, Y. M.; Kim, K. K.; Reina, A.; Hofmann, M.; Li, L. J.; Kong, J. *ACS Nano* **2010**, *4*, 2689–2694.
(29) Riviere, J. C. *Solid State Surface Science*; Decker: New York, 1969.
(30) Sharma, B. L. *Metal-Semiconductor Schottky Barrier Junctions and Their Applications*; Plenum Press: New York, 1984.
(31) Zhang, L. H.; Jia, Y.; Wang, S. S.; Li, Z.; Ji, C. Y.; Wei, J. Q.; Zhu, H. W.; Wang, K. L.; Wu, D. H.; Shi, E. Z.; Fang, Y.; Cao, A. Y. *Nano Lett.* **2010**, *10*, 3583–3589.
(32) Wang, X. R.; Li, X. L.; Zhang, L.; Yoon, Y.; Weber, P. K.; Wang, H. L.; Guo, J.; Dai, H. J. *Science* **2009**, *324*, 768–771.
(33) Wu, C. Y.; Chen, J. F. *J. Appl. Phys.* **1982**, *53*, 3852–3858.
(34) Snaith, H. J.; Schmidt-Mende, L.; Grätzel, M. *Phys. Rev. B* **2006**, *74*, 045306.

AM1007672